Supporting Information for "Vertical structure in phytoplankton growth and productivity inferred from Biogeochemical-Argo floats and the Carbon-based Productivity Model"

Lionel A. Arteaga[1,2,3], Michael J. Behrenfeld[4], Emmanuel Boss[5], Toby K. Westberry[4]

[1]Global Modeling and Assimilation Office, NASA Goddard Space Flight Center, Greenbelt, MD 20771, USA

[2]Goddard Earth Sciences, Technology and Research II, University of Maryland Baltimore County, Baltimore, MD 21250, USA

[3]Program in Atmospheric and Oceanic Sciences, Princeton University, 300 Forrestal Rd, Princeton, NJ, USA

[4]Department of Botany and Plant Pathology, Oregon State University, Cordley Hall 2082, Corvallis, OR 97331-2902, USA

[5]School of Marine Sciences, University of Maine, 5706 Aubert Hall, Orono, ME 04469-5741, USA

Contents of this file

1. Figures S1 to S5

2. Tables S1

Introduction

This supporting material contains a map showing the global distribution of BGC-Argo float profiles with vertically-resolved estimates of net primary production from the various implementations of the CbPM (Figure S1). Also shown are fully vertically-resolved (within and below the mixed layer) NPP profiles from the $CbPM_{Argo}$ against depth-resolved in situ ^{14}C-based observations of productivity from the Arabian Sea (Figure S2).

Seasonally-averaged Chl:C and phytoplankton carbon (C_{phyto}) profiles near the ALOHA station (profiles sampled between 22°N – 23°N, and 157°W – 159°W), obtained from in situ observations, the bio-optical float sensors ($CbPM_{Argo}$) (Argo), inferred by the float-based $CbPM_{Orig}$ (Orig), and $CbPM_{Mod}$ (Mod), and satellite-based $CbPM_{Sat}$ (informed by satellite ocean color inputs) are presented (Figure S3). Seasonally-averaged Chl:C and C_{phyto} from the float data ($CbPM_{Argo}$) and float-based CbPM implementations ($CbPM_{Orig}$ and $CbPM_{Mod}$) are also presented for the Southern Ocean between 40°S and 50°S (Figure S4).

The relationship between float-based mean Chl:C ratio (gr gr^{-1}) in the upper mixed layer and the median mixed layer light level (E m^{-2} d^{-1}) inferred from the spectral component of the $CbPM_{Argo}$ is shown (Figure S5). Details of stations/cruises from the Marra et al. (2021) dataset where in situ measurements and float-based productivity profiles where obtained and compared are provided (Table S1).

References

Marra, J. F., Barber, R. T., Barber, E., Bidigare, R. R., Chamberlin, W. S., Goericke, R., ... Zoffoli, L. (2021). A database of ocean primary productivity from the 14c method. *Limnology and Oceanography Letters*, *n/a*(n/a). Retrieved from `https://aslopubs.onlinelibrary.wiley.com/doi/abs/10.1002/lol2.10175` doi: https://doi.org/10.1002/lol2.10175

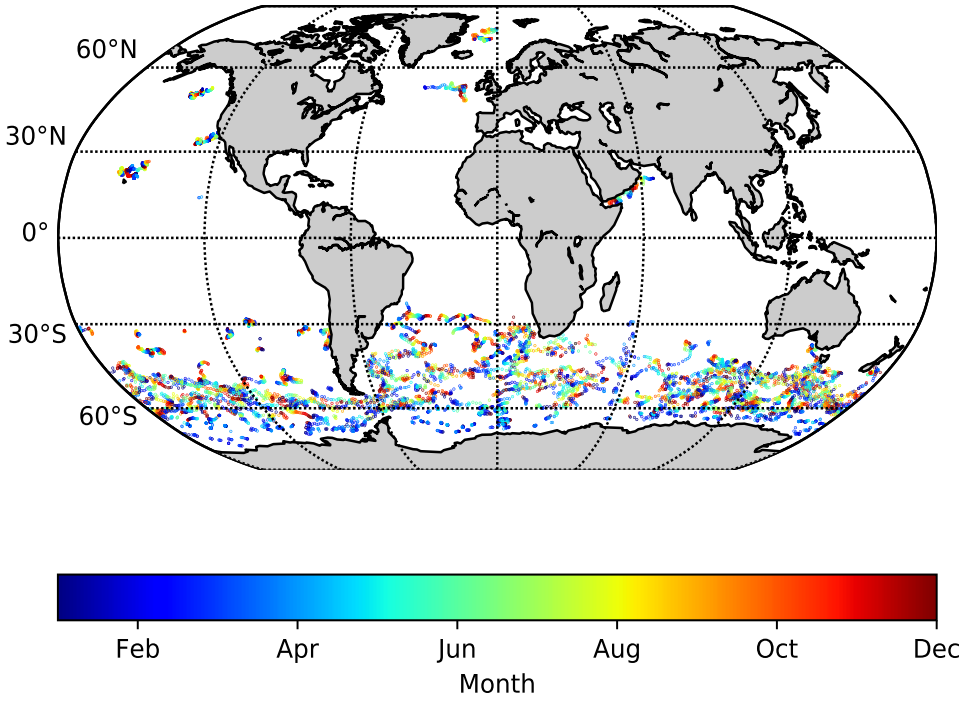

Figure S1. Global distribution of BGC-Argo float profiles with vertically-resolved estimates of net primary production from the various implementations of the CbPM. The colormap indicates the month in which each profile was sampled.

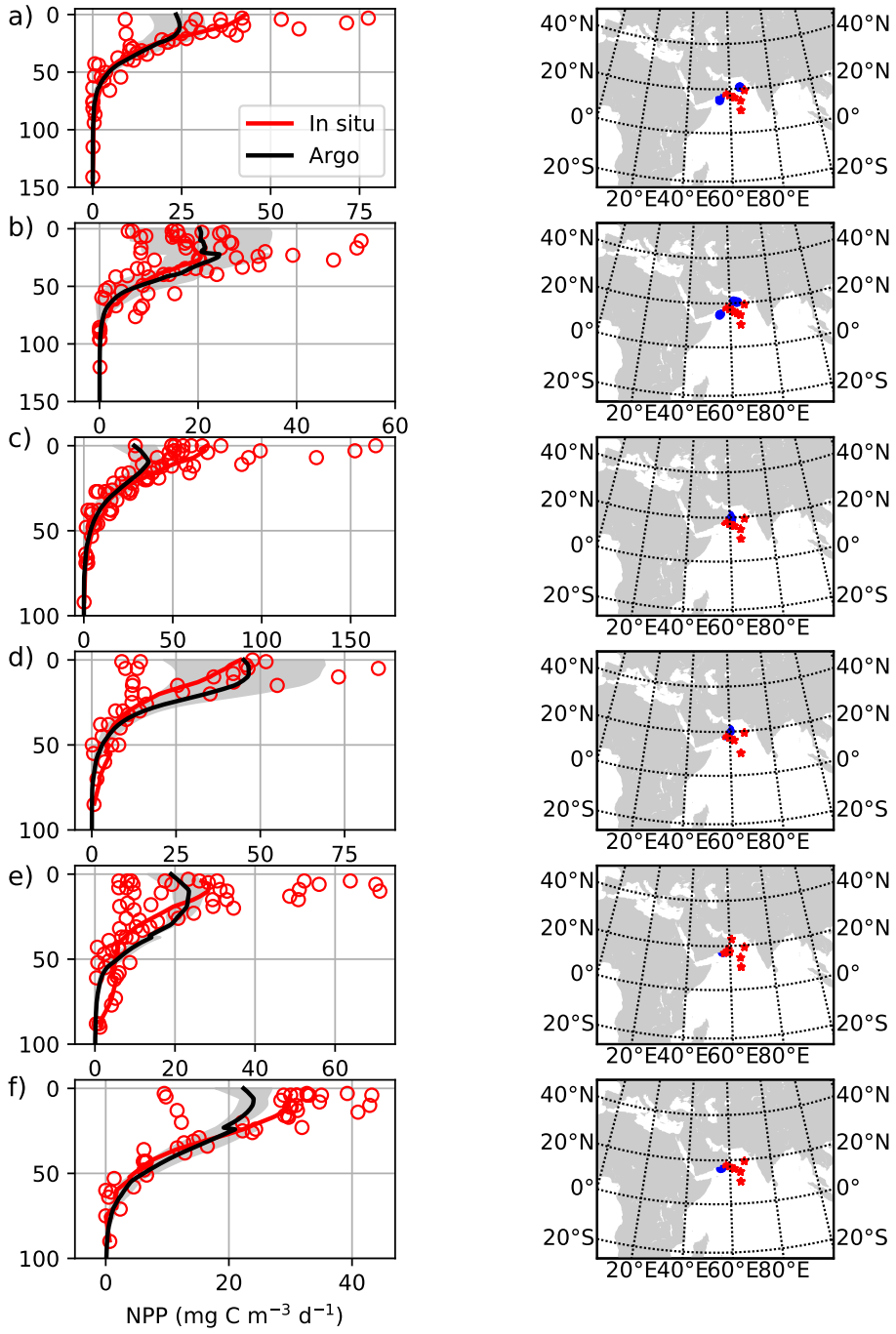

Figure S2. (left panels) In situ ^{14}C-based NPP measurements (open red circles) and averaged float-based NPP profiles obtained from the CbPM$_{\text{Argo}}$ (black line ± standard deviation represented by the gray-shaded area). Red line represents the average of depth-interpolated in situ profiles. (right panels) Geographical location of in situ ^{14}C-based productivity profiles (red filled circles) and float NPP profiles (blue filled circles) for stations (cruise designation) in the Arabian Sea: (a) ttn-043, (b) ttn-045, (c) ttn-049, (d) ttn-050, (e) ttn-053, (f) ttn-054 (See Table S1 for specific details of each cruise/station).

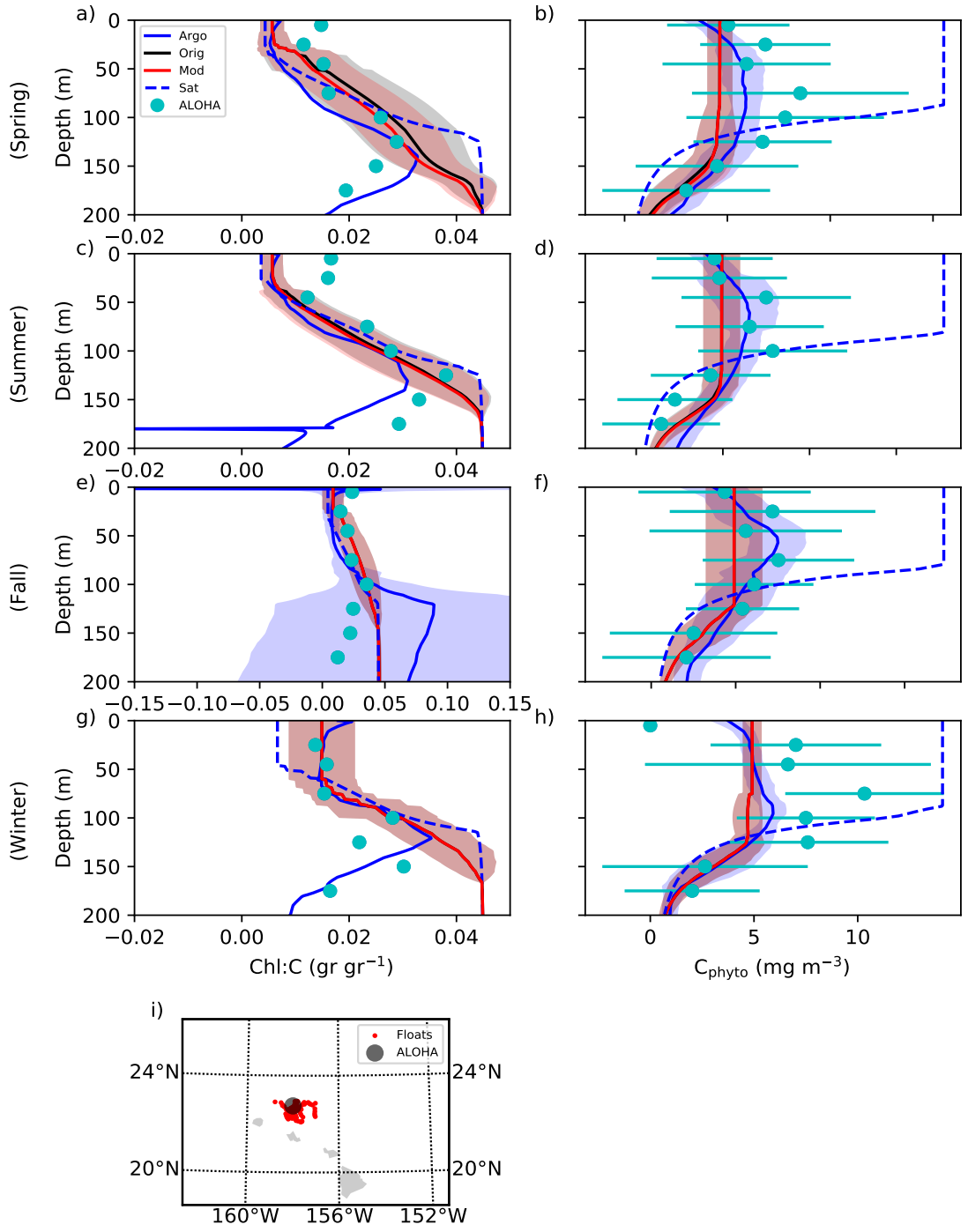

Figure S3. Seasonally-averaged Chl:C ratio (gr gr^{-1}) (left column) and C_{phyto} (mg C m^{-3}) (right column) profiles near station ALOHA for (a-b) Spring, (c-d) Summer, (e-f) Fall, (g-h) Winter (boreal seasons). Profiles are obtained from the $CbPM_{Argo}$ (Argo, solid blue line), $CbPM_{Orig}$ (Orig, solid black line), $CbPM_{Mod}$ (Mod, solid red line), $CbPM_{Sat}$ (Sat, dashed blue line), and in situ observations (ALOHA, solid cyan circles ± standard deviation). Shaded areas represent ± standard deviation of the float-based model implementations. (i) Location of float profiles (red) and in situ field station (dark grey).

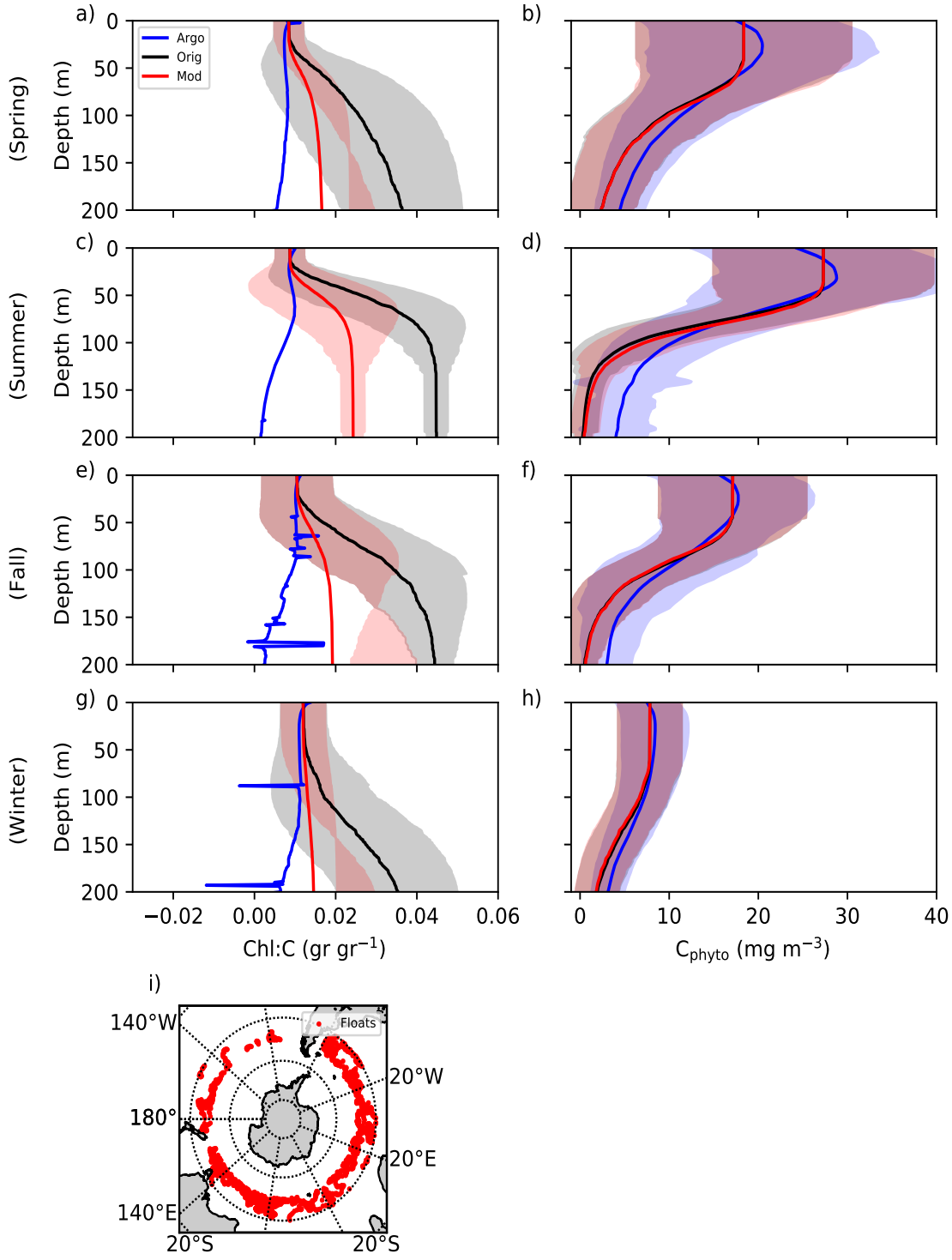

Figure S4. Seasonally-averaged Chl:C ratio (gr gr^{-1}) (left column) and C_{phyto} (mg C m^{-3}) (right column) profiles in the Southern Ocean between 40°S and 50°S for (a-b) Spring, (c-d) Summer, (e-f) Fall, (g-h) Winter (austral seasons). Profiles are obtained from the $CbPM_{Argo}$ (Argo, solid blue line), $CbPM_{Orig}$ (Orig, solid black line), and $CbPM_{Mod}$ (Mod, solid red line). Shaded areas represent ± standard deviation of the float-based model implementations. (i) Location of float profiles (red).

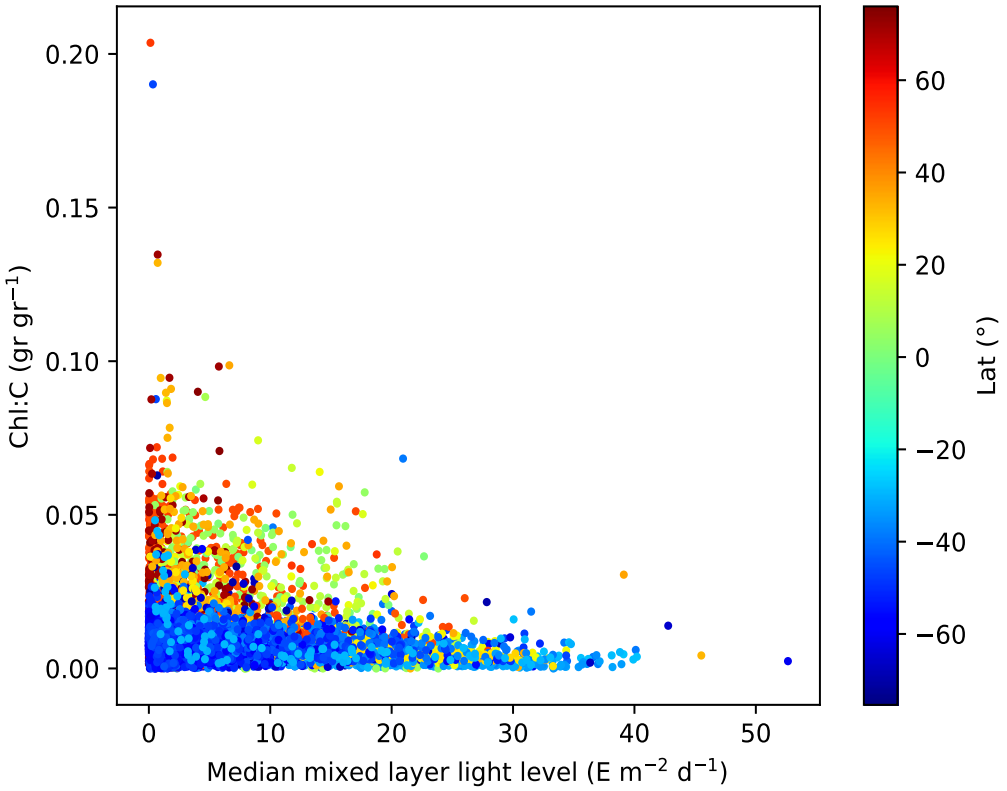

Figure S5. Scatter plot of mean Chl:C ratio (gr gr^{-1}) in the upper mixed layer from BGC-Argo float profiles and median mixed layer light level (E m^{-2} d^{-1}) inferred from the spectral component of the CbPM$_{\text{Argo}}$.

Table S1. Oceanic region, station (cruise designation and year), geographical limits, and months where BGC-float productivity profiles from the $CbPM_{Argo}$ and in situ depth-resolved ^{14}C-based NPP observations from Marra et al. (2021) were obtained and compared. The region name and cruise designation are shown as defined in the original compiled data set. Also shown are the SOCCOM ID of floats in each comparison, years when profiles were obtained from each float(s) and total number of profiles matched.

Region	Cruise designation (year)	Geographical coordinates (°)	Months	Float matchups SOCCOM ID (years)	Profiles
Ross Sea	NBP-97-1; (1997)	78S–70S; 170E–160W	Jan–Mar	7614 (2018) 12363, 12381, 12541 (2018-2019) 12398, 12758 (2020)	26
Polar Front	rr-kiwi-7; (1997)	77S–53S; 175E–164W	Dec	6091 (2014–2016) 0566, 0570, 0571, 7620 (2016) 12388 (2017), 12701 (2018) 12736, 12779, 12784 (2019)	29
	rr-kiwi-9; (1997)	77S–53S; 175E–164W	Feb-Mar	6091 (2015–2017), 7620 (2017) 12388 (2018) 12541, 7614 (2018–2019) 12701 (2018-2020) 12736, 12758, 12779, 12784 (2020)	69
North Pacific Gyre	Alcyone-III; (1985)	20N–30N; 157W–150W	Aug–Sep	17267, 17307 (2019), 8486 (2013)	37
Sub-Arctic North Atlantic	EN 224; (1991)	50N–60N; 25W–20W	May	0276 (2014–2015)	7
	EN 227; (1991)	50N–60N; 25W–20W	Aug	0276 (2014)	5
Arabian Sea	ttn-043; (1995)	8N–24N; 55E–70E	Jan	6381 (2012–2013)	8
	ttn-045; (1995)	8N–24N; 55E–70E	Mar–Apr	6381 (2012–2013)	12
	ttn-049; (1995)	8N–24N; 55E–70E	Jul–Aug	6381 (2012)	8
	ttn-050; (1995)	8N–24N; 55E–70E	Aug-Sep	6381 (2012)	8
	ttn-053; (1995)	8N–24N; 55E–70E	Nov	6381 (2012)	6
	ttn-054; (1995)	8N–24N; 55E–70E	Dec	6381 (2012)	5

Corresponding float WMO number in brackets: 12363 (5905102), 12381 (5904857), 12398 (5905638), 12541 (5904860), 12758 (5905637), 7614 (5904183), 0566 (5904766), 0570 (5904768), 0571 (5904673), 12388 (5905099), 12701 (5905635), 12736 (5905376), 12779 (5905371), 12784 (5905372), 6091 (5904179), 7620 (5904104), 17267 (5906039), 17307 (5906040), 8486 (5904124), 0276 (5904479), 6381 (5903586).